JOURNAL OF SPACECRAFT AND ROCKETS
Vol. 32, No. 1, January–February 1995

Fuel-Optimal Bank-Angle Control for Lunar-Return Aerocapture

J. L. Meyer,* L. Silverberg,† and G. D. Walberg‡
North Carolina State University, Raleigh, North Carolina 27695-7921

Aerocapture is defined as the deceleration of a spacecraft due to drag produced on it by a planet's atmosphere such that the vehicle is captured into orbit about the planet. This is accomplished by varying the direction of the vehicle's lift vector through bank-angle modulation. This paper examines the application of four optimal-control approaches to aerocapture. The first is a minimization of a pseudo fuel cost function, which yields continuous controls. The second is bang-bang control, which minimizes the time associated with bank-angle modulation. Next, an absolute fuel function is minimized, which results in controls in the form of impulses. A fourth approach is a modification to impulsive control, where impulses are approximated by pulses of finite duration. All of the approaches are applied to a single-pass aerocapture problem. The modified impulsive-control approach is applied to a two-pass aerocapture scenario. Recommendations on the practical implementation of these control approaches in the presence of vehicle and atmospheric uncertainties are given.

Nomenclature

c	= $N \times 1$ vector of impulse coefficients
$E(t)$	= represents rotational energy of the spacecraft, $\frac{1}{2} I_\phi \Omega_\phi^2(t)$, N-m
e^{-At}	= state transition matrix
Fu*	= minimum fuel, $1/\zeta^*$, N-m-s
H	= hyperplane
I_α, I_β, I_ϕ	= mass moments of inertia about the respective angles, kg-m^2
R	= control weight, s^2
sgn(·)	= sign function
t_0	= initial control time, s
t_f	= final control time, s
$u_{\max}$	= maximum producible control torque, N-m
u_ϕ	= control torque about the velocity vector, N-m
x_0	= $x(t_0)$
x_f	= $x(t_f)$
y	= reachable state
α, β, ϕ	= angle of attack, sideslip angle, and bank angle, deg
δ	= error reduction coefficient
Δ	= $N \times 1$ vector of impulses
κ	= user-defined design parameter, s^{-1}
Ω_α, Ω_β, Ω_ϕ	= rotation rates about the respective angles, deg/s
η	= 2×1 vector
ζ^*	= fuel coefficient, N^{-1}-m^{-1}-s^{-1}

Introduction

WITH the interest in economizing interplanetary missions, there has been a renewed emphasis on the concept of aerocapture. Aerocapture is defined as the deceleration of a spacecraft due to drag produced on it by a planet's atmosphere such that the vehicle is captured into orbit about the planet. Aerocapture has been extensively studied,[1–5] and its advantages over propulsive deceleration have been documented. Aerocapture, as opposed to chemical propulsive deceleration, has been shown to reduce mission fuel requirements by as much as 20–40%. The object of aerocapture is usually to pass through the attracting planet's atmosphere and place the vehicle in a targeted elliptical orbit from which a subsequent rocket burn will produce the desired parking orbit. The trajectory entry corridor is defined by an upper and lower threshold depending on the planet's atmosphere and the vehicle's velocity and aerodynamic characteristics.[6] With hyperbolic entry velocities, the differences among the admissible inertial-flight-path angles at the atmospheric interface, which dictate the upper and lower thresholds, are small. The entry restrictions are particularly severe in an Earth aeropass, because of the high planetary surface gravity and the resultant small scale height of the atmosphere.[7] The bounds of the entry corridor are altered by mission requirements and vehicle design limitations to yield the flyable corridor.[8–10] The undershoot bound is defined by the steepest trajectory that can be flown and still achieve the target orbit. The overshoot bound is the shallowest trajectory that can be flown, constrained by peak deceleration and/or thermal loading restrictions, and achieve the target orbit. If atmospheres were static in nature, the corridor would be easily defined and a simple ballistic trajectory could be flown, assuming a precise entry angle for the vehicle. However, in the presence of atmospheric variations, aerodynamic mispredictions, and limitations in interplanetary navigation accuracy, the location and size of the flyable corridor can be greatly influenced.[11] Without proper aerodynamic control of the vehicle, the chances of achieving the target orbit while remaining within the vehicle constraints are greatly reduced. In order to ensure successful aerocapture, modulation of the lift vector must be incorporated into the guidance system. This is usually implemented through feedback control of the bank angle as seen in Fig. 1. The ability to modulate expands the entry corridor.[12]

In an extension of a single aeropass to achieve the necessary energy decrement, the concept of multipass aerocapture has been suggested.[13] A decrease in g loading and peak heating rate can be achieved by spreading the energy dissipation over multiple passes. An additional benefit is the reduced velocity change required to circularize the target orbit after the final pass.

Various approaches for feedback control of spacecraft during aerocapture have been studied. Some approaches implemented control about a path defined by certain nominal trajectory characteristics.[14–16] Other approaches have employed displacement and velocity feedback schemes augmented with predictor-corrector algorithms to compensate for atmospheric, aerodynamic, and navigational uncertainties.[17–19] Approximate optimal-control approaches have been examined for aeroassisted plane-change maneuvers and aerocapture.[20,21]

This paper examines the application of three optimal-control approaches to aerocapture. The first is a minimization of a pseudo fuel cost function, which yields continuous controls that are suited to control moment gyros, torque wheels, or throttlable reaction control jets. The second minimizes the time associated with bank-

Received July 8, 1993; revision received May 16, 1994; accepted for publication May 24, 1994.

*Graduate Research Assistant, Mars Mission Research Center. Student Member AIAA.

†Associate Professor, Mechanical and Aerospace Engineering. Member AIAA.

‡Professor, Mechanical and Aerospace Engineering. Fellow AIAA.

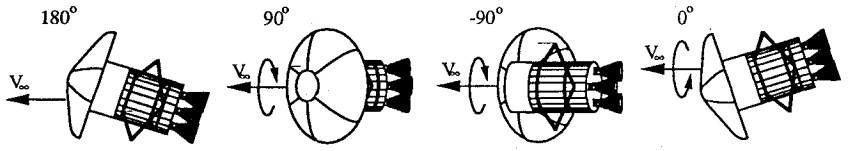

Fig. 1 Aeropass bank-angle control.

angle modulation and yields bang-bang controls that are suited to propulsive actuators. Propulsive actuators are also suited by the third approach, which minimizes the absolute fuel function and yields controls in the form of impulses. This approach is termed fuel-optimal control. A fourth approach, which is a modification to fuel-optimal control where impulses are approximated by pulses of finite duration, is similar to the atmospheric guidance algorithms implemented on Viking.[22] In previous studies, designers have evaluated the performance of control approaches with respect to trajectory characteristics. The optimal-control approaches presented here are evaluated with respect to the g loading, heating rate, and total heating during an ideal aerocapture.

Aerocapture Maneuvers

In order to assess their merits, the optimal-control approaches mentioned above were applied to a lunar-return aerocapture vehicle. The vehicle configuration is shown in Fig. 2, and its parameters are presented in Table 1. The aerobrake has a diameter of 15.24 m, a spherical-nose radius of 3.39 m, an edge radius of 0.34 m, and a cone half-angle of 70 deg. The aerobrake geometry is essentially that of the Viking aeroshell, and the vehicle is patterned after the "single-propulsion avionics module" lunar transfer-vehicle concept studied by the NASA Marshall Space Flight Center. The vehicle has an all-up Earth-return mass of 19,457 kg. It flies at a constant angle of attack of 10 deg and has a drag coefficient of 1.51 and a lift coefficient of 0.254. Hence, it has an L/D of 0.168 and a ballistic coefficient of 70.6 kg/m^2.

The velocity at entry into the Earth's atmosphere (assumed to occur at 130 km) was 11 km/s with the vehicle in a planar trajectory inclined to the equator by 28.5 deg. The aerocapture maneuvers consisted of a series of bank-angle modulations targeted to place the vehicle in an elliptic orbit with an apogee altitude of 500 km on exit from the atmosphere. A final circularization burn, carried out at apogee, placed the vehicle in a circular parking orbit that had an altitude of 500 km and an inclination of 28.5 deg.

Both single-pass and two-pass aerocapture maneuvers were investigated. In the single-pass scenario, the bank angles were optimized to minimize the velocity change ΔV required for orbit circularization. In the two-pass scenario, the bank angles for the first pass were optimized to minimize the peak convective aerodynamic heating rate while placing the vehicle in a 6-h, 28.5-deg intermediate orbit. The second-pass bank angles were optimized to minimize the ΔV required for final circularization. All trajectory calculations were carried out using the Program to Optimize Simulated Trajectories (POST) algorithm.[23]

An initial set of calculations was carried out to establish the entry corridors for the single-pass and two-pass scenarios. The overshoot bounds were established by flying a constant 180-deg (lift down) bank angle and determining the smallest entry flight-path angle that would yield the desired orbit on exit from the atmosphere. The undershoot bounds were established by flying a constant 0-deg (lift up) bank angle. For the single-pass scenario, the undershoot bound corresponded to the entry flight-path angle that produced a peak deceleration of $5g$. For the two-pass scenario, the undershoot bound corresponded to the steepest entry flight-path angle that would yield the required 6-h intermediate orbit. The entry corridor was bounded by entry flight-path angles of -5.01 and -5.81 deg for the single-pass scenario and -4.90 and -5.16 deg for the first pass of the two-pass scenario. Once the entry corridors had been established, midcorridor reference trajectories were computed wherein the idealized bank-angle modulations were represented by step functions. The entry angle was -5.29 deg for the idealized single-pass scenario. For the idealized two-pass scenario, the entry angles were -5.043 and -4.327 deg for the first and second passes respectively.

Table 1 Vehicle parameters

Parameter	Value
Mass	19457 Kg
I_ϕ	68682 kg-m^2
Nose radius	3.39 m
Ref. diameter	15.24 m
Ref. area	182.4 m^2
AOA α	-10.0 deg
C_L	0.254
C_D	1.51
$m/(C_D A)$	70.6 kg/m^2

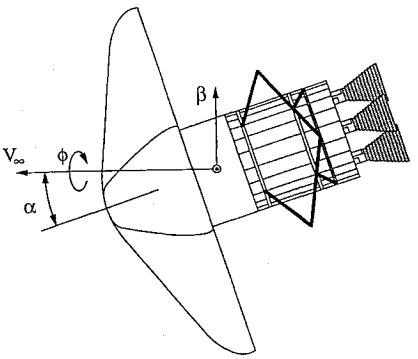

Fig. 2 Vehicle coordinate system.

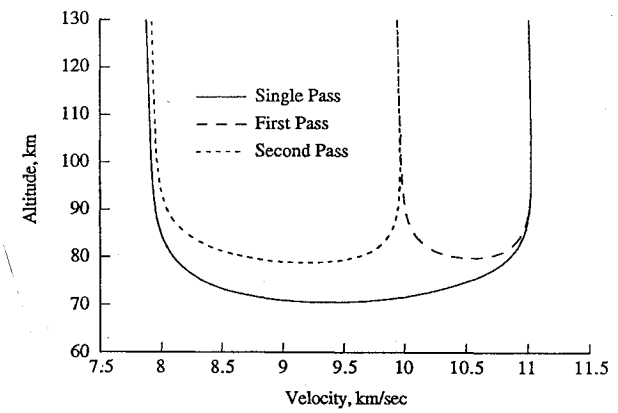

Fig. 3 Aeropass velocity-altitude time histories.

The velocity-altitude histories for these reference trajectories are presented in Fig. 3, and the corresponding stagnation-point aerodynamic heating-rate time histories are presented in Figs. 4a and 4b. The 1967 U.S. Standard Atmosphere was used in all calculations.[24] Convective heating rates were computed using Chapman's equation and assuming a cold wall and chemical equilibrium. Radiative heating rates were estimated using inviscid equilibrium solutions.[25,26] Note that the minimum altitudes for the two-pass trajectories are significantly higher than those for the single-pass. As a result, the peak decelerations (and hence the aerodynamic loads) are markedly reduced. There are also important reductions in both convective and radiative heating rates, as shown in Fig. 4. Also, the ΔV required to circularize the final 500-km-altitude parking orbit was significantly decreased from the single-pass case. The lower decelerations would allow a lighter aerobrake structure. Note, in a related, but unpublished, Mars Mission Research study of the aerobraking vehicle analyzed in this paper, that the structural weight savings due to the lower

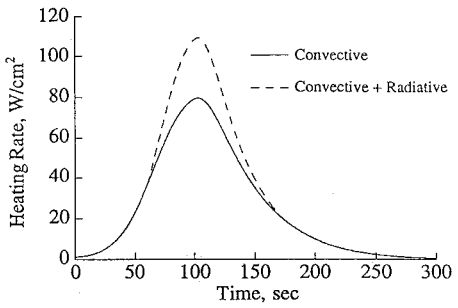

Fig. 4a Single-pass heating rates.

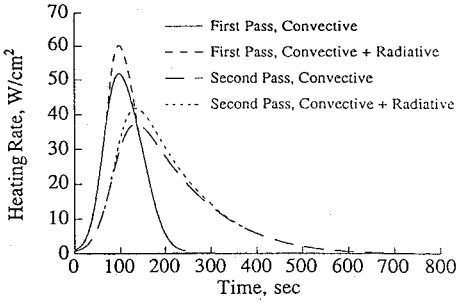

Fig. 4b Two-pass heating rates.

decelerations far exceeded the weight increase due to the thicker heat shield. The reduced heating rates are low enough to allow a reusable heat shield. The reduced ΔV requirement would allow significant savings in propellant mass. These idealized trajectories served as a starting point for the optimal-control simulations presented in the following sections. The advantages just mentioned for the two-pass scenario are also obtained when optimal-control approaches are employed.

Spacecraft Dynamics

The rotational dynamics of the spacecraft about its velocity vector V_∞ are represented by the differential equation (Fig. 2)

$$I_\phi \frac{d\Omega_\phi}{dt} - (I_\alpha - I_\beta)\Omega_\alpha \Omega_\beta = u_\phi \tag{1}$$

In this analysis the control torque is applied entirely about the velocity vector, the brake is symmetric, and atmospheric perturbations are assumed to be negligible, so that $\Omega_\alpha \Omega_\beta \approx 0$.

Equation (1) is recast in the form of the first-order linear state equations

$$\dot{x}(t) = Ax(t) + Bu_\phi(t)$$
$$A = \begin{bmatrix} 0 & 1 \\ 0 & 0 \end{bmatrix}, \qquad B = \begin{bmatrix} 0 \\ 1/I_\phi \end{bmatrix} \tag{2}$$

where $x(t) = [\phi \quad \Omega_\phi]^T$.

Formulation of the Control Problems

The following describes three optimal-control problems. The objective in each case is to transfer the system from some initial orientation ϕ_0 to a final orientation ϕ_f while minimizing a given cost function. The first case is for continuous control, the second is for bang-bang control, and the third is for impulsive control. A fourth problem is also presented in which the impulsive control is modified to yield a bang-off-bang control.

Continuous Control

The continuous control is obtained from the minimization of the quadratic cost function[27]

$$C_c = \int_{T_0}^{\infty} \left[E(t) + Ru_\phi^2(t)\right] dt \tag{3}$$

where $R = (2\kappa^2)^{-1}$. The minimization of C_c leads to the continuous control (state feedback)

$$u_\phi(t) = -\kappa^2 I_\phi \phi(t) - 2\kappa I_\phi \Omega_\phi(t) \tag{4}$$

where $\kappa = -(\ell n \delta)/(t_f - t_0)$ [e.g., if it is desired to reduce the bank angle error by 95% within the control time, then $\delta = (100-95)/100 = 0.05$]. Continuous control is normally realized by control moment gyros, torque wheels, or throttlable reaction control jets.

Bang-Bang Control

Next we define a control that is based on the minimization of the largest control input and whose cost function is[28]

$$C_b = \sup_{t_0 \le t \le t_f} |u_\phi(t)| \tag{5}$$

The minimization of this cost function yields the minimum-time bang-bang control

$$u_\phi(t) = \begin{cases} u_{\max} \operatorname{sgn}\left(\dfrac{\phi_f - \phi_0}{2} - \phi(t)\right), & \phi_0 \le \phi(t) < \phi_f \\ 0 & \text{otherwise} \end{cases} \tag{6}$$

Impulsive Control

Impulsive control results from the minimization of the absolute fuel that is associated with propulsive actuation. The fuel-optimal cost function[29-31] is

$$C_i = \int_{t_0}^{t_f} |u_\phi(t)|\, dt \tag{7}$$

The control determining function is defined as $g(\eta, t) = \eta^T e^{-At} B$, where η is contained in H, $H = (\eta : \eta^T y = 1)$, $y = e^{-At_f} x_f - x_0$, and

$$e^{-At} = \begin{bmatrix} 1 & -t \\ 0 & 1 \end{bmatrix}.$$

The solution to the fuel-optimal-control problem is determined by selecting η such that

$$\zeta^* = \min_{\eta \in H} \sup_{t_0 \le t \le t_f} |g(\eta, t)| \tag{8}$$

The solution to Eq. (8) yields the optimal normal vector η^*, resulting in a control of the form

$$u^*(t) = \frac{\Delta^T c}{\zeta^*} \tag{9a}$$

where Δ and c are given by

$$\Delta = [\operatorname{sgn} g(\eta^*, \tau_1)\, \delta(t - \tau_1) \quad \cdots \quad \operatorname{sgn} g(\eta^*, \tau_N)\, \delta(t - \tau_N)]^T \tag{9b}$$

$$c = [c_1 \quad c_2 \quad \cdots \quad c_N]^T \tag{9c}$$

where $\delta(t - \tau_i)$ is a unit impulse at time τ_i. The impulse coefficients are nonnegative constants that satisfy $1 = \Sigma_{i=1}^N c_i$.

The control determining function for the spacecraft bank-angle maneuver is

$$g(\eta, t) = -\frac{t}{I_\phi}\eta_1 + \frac{1}{I_\phi}\eta_2 \tag{10}$$

The bank-angle maneuver is defined by $x_0 = [\phi_f - \phi_0 \quad 0]^T$ and $x_f = 0$, which, after imposing the hyperplane constraint, yields $\eta_1 = -1/(\phi_f - \phi_0)$. By inspection of Eqs. (8) and (10), it can be determined that

$$\eta = \left[-\frac{1}{\phi_f - \phi_0} \quad -\frac{t_f - t_0}{2(\phi_f - \phi_0)}\right]^T, \qquad \zeta^* = \left|\frac{t_f - t_0}{2I_\phi(\phi_f - \phi_0)}\right| \tag{11}$$

The solution to the fuel-optimal bank-angle control problem yields $N = 2$, for which $\tau_1 = t_0$ and $\tau_2 = t_f$.

The impulse coefficients are determined next. The solution to Eq. (2) is given by

$$x(t) = e^{At}\left(x(t_0) + \int_{t_0}^{t} e^{-As}Bu(s)\,ds\right) \tag{12}$$

Substituting Eq. (9) into Eq. (12) evaluated at time t_f results in a set of simultaneous linear-algebraic equations given by

$$Pc = Q$$

$$Q = \begin{bmatrix} y \\ 1 \end{bmatrix}, \qquad P = \begin{bmatrix} \dfrac{1}{\zeta^*}\displaystyle\int_{t_0}^{t_f} e^{-At}Bg^T\,dt \\ 1 \end{bmatrix}, \qquad c = \begin{bmatrix} c_1 \\ c_2 \end{bmatrix} \tag{13}$$

In the case of fuel-optimal bank-angle control, the solution to Eq. (13) results in $c_1 = c_2 = \frac{1}{2}$.

Modified Impulsive Control (Bang-Off-Bang)

Impulsive control is impossible to implement exactly. In practice the instantaneous impulses must be converted into finite-time pulses of duration Δt. Equating the magnitudes of the impulse and of the finite-duration pulse yields[32]

$$\int_{T_{1i}}^{T_{2i}} u_{\phi i}\,dt = \int_{T_{1i}}^{T_{2i}} \frac{c_i}{\zeta^*}\operatorname{sgn} g(\eta^*, \tau_i)\,\delta(t - \tau_i)\,dt = \frac{c_i}{\zeta^*} \tag{14}$$

$$T_{2i} - T_{1i} = \Delta t_i = \frac{c_i}{\zeta^* u_i} \tag{15}$$

This results in a pulse of duration Δt_i and of magnitude u_i, corresponding to the ith impulse in the solution to the fuel-optimal-control problem. Equating impulse and pulse magnitudes reveals implications associated with the controller design. The first of these results is that the coast angular velocities Ω_ϕ are identical for impulsive control and for modified impulsive control. Secondly, the maneuver times for the modified impulsive approach are slightly larger than those for impulsive control, by $\Omega_\phi/\dot{\Omega}_\phi$. Finally, the fuels associated with each approach for maneuvers of equal magnitude are identical.

Simulation Results

The control approaches were simulated using the three-degree-of-freedom version of POST.[23] POST is a general-purpose FORTRAN program that simulates and optimizes point-mass trajectories for a variety of aerospace vehicles. All trajectory simulations were segmented into six phases, with the first maintaining a constant bank angle for 50 s, which corresponded to a period of minimal aerodynamic control authority. The next four phases were each 25 s in duration and corresponded to the region where the bank-angle control sequence was implemented. The final phase lasted until the defined termination conditions in the trajectory were achieved.

Single-Pass Aerocapture

For each of the single-aeropass simulations presented, the entry velocity was 11 km/s and the entry altitude was 130 km. The entry flight-path angle γ was -5.287 deg, which corresponded to a mid-corridor trajectory. The orientation of the vehicle was defined by an angle of attack of -10 deg and a sideslip angle of 0 deg.

The goal of the aeropass was to target exit conditions that would place the vehicle in an elliptical orbit with an apogee altitude of 500 km and an inclination angle of 28.5 deg. The aeropass was optimized so that the ΔV required for circularization at the 500-km apogee of the targeted orbit was minimized. Towards this end, the closed-loop control algorithms were incorporated into the POST software. The resulting control-dependent bank angles used a commanded bank-angle sequence as feedback. POST then optimized the commanded bank-angle sequence with respect to the dynamics of the closed-loop system so that the appropriate atmospheric exit conditions were obtained. Figure 5 shows the resulting bank-angle sequences of the four control approaches along with the step-function, or ideal, bank-angle sequence. The ideal sequence assumed that an instantaneous change in bank angles was possible. Note that while the general patterns of the sequences are similar, the closed-loop bank-angle magnitudes have been modified. In the case of continuous control, κ was chosen such that the bank-angle error was reduced by 95% within 10 s of t_0. For bang-bang control, an acceleration rate of 5 deg/s^2 was assumed. For impulsive control, a finite rotation rate of 15 deg/s was selected. In the modified impulsive-control approach, a pulse accelerated the bank-angle rotation at 5 deg/s^2 until the vehicle achieved a 15 deg/s rate. The vehicle was then allowed to coast until an equivalent deceleration pulse brought it to rest at the commanded bank angle. Note that all optimized bank-angle profiles were successful in obtaining the prescribed parking orbit. However, in the interest of brevity, only the modified impulsive control approach is compared with the ideal profile in the subsequent illustration.

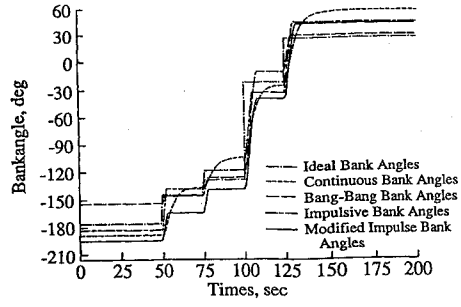

Fig. 5 Single-pass bank-angle histories.

Figures 6a–6c compare the dynamics and heating characteristics of the modified impulsive-control approach to the ideal bank-angle profile. In each of the flight characteristics examined in Fig. 6, the modified impulsive-control dynamics are quite similar to the ideal case. The vehicle decelerations range between $4.41g$ and $4.65g$, which is the peak associated with the ideal case. The convective heating rates range between 77.78 and 79.68 W/cm^2, and the convective heat load is in the vicinity of 7600–7800 J/cm^2. It should be emphasized that with regard to the heating rates and total heat, there was no significant penalty when the optimal-control approaches were implemented. This was also true in reference to the ΔV required for orbit circularization, which ranged from 157 to 167 m/s.

A question arises as to what effect feedback control about the ideal bank-angle sequence has on the trajectory. Unfortunately, the aeropass is extremely sensitive to the vehicle bank-angle profile, to the extent that deviations result in failure to reach the desired atmospheric exit state. Figure 7 illustrates the results of controlling about the ideal bank-angle sequence using the continuos, bang-bang, and impulsive-control approaches. The ideal sequence is the result of an optimization assuming instantaneous changes in bank angles. In each case, the vehicle did not achieve the targeted exit conditions and atmospheric capture resulted. This reveals the importance of optimizing the vehicle's bank-angle sequence with respect to the intended control methodolgy.

Fuel Comparison

An examination of the fuel requirements for each of the control approaches is now presented as a function of the design parameters associated with each. Each control is compared on the basis of absolute fuel, which is defined as

$$\mathrm{Fu} = \int_{t_0}^{t_f} |u_\phi(t)|\,dt \tag{16}$$

A unit-step (1 rad) rest-to-rest maneuver is used as the basis for comparing the fuel consumed in the four control approaches. Closed-form solutions for the fuel in each case are

$$\mathrm{Fu}_c = 2\kappa I_\phi e^{-1}, \qquad \mathrm{Fu}_b = 2I_\phi\sqrt{\dot{\Omega}_\phi}, \qquad \mathrm{Fu}_i = \mathrm{Fu}_m = 2I_\phi\Omega_\phi \tag{17}$$

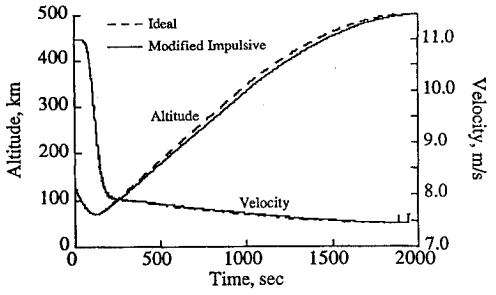

Fig. 6a Altitude and velocity history, single pass.

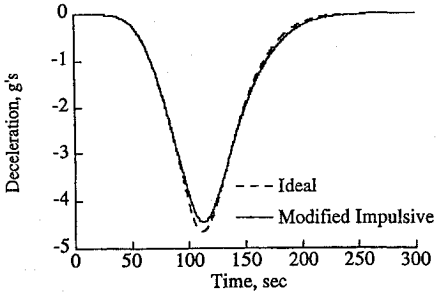

Fig. 6b Deceleration history, single pass.

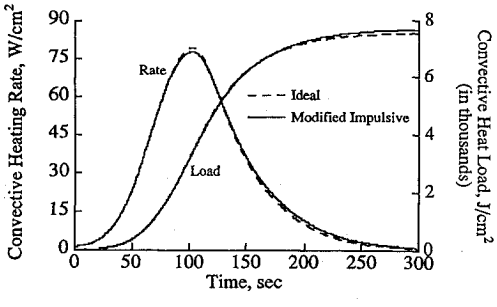

Fig. 6c Convective heating rate, single pass.

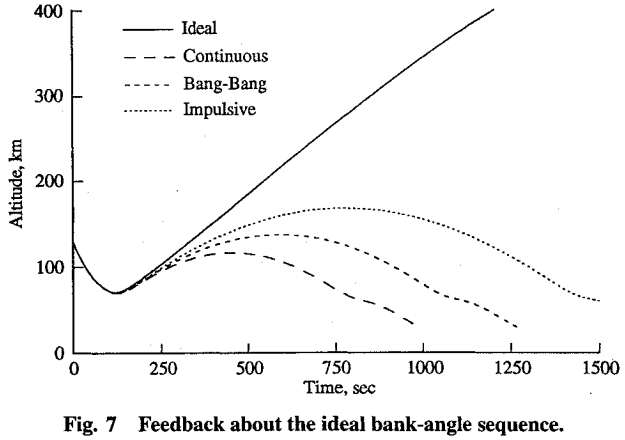

Fig. 7 Feedback about the ideal bank-angle sequence.

where Fu_c, Fu_b, Fu_i, and Fu_m are the fuels associated with continuous, bang-bang, impulsive, and modified impulsive controls, respectively. Note that the fuels associated with impulsive and modified impulsive controls are identical, which results from the pulse width determination in Eq. (15). Figure 8 compares the fuels required for the unit-step maneuver for each control approach. One point to consider is that for the same maneuver time, the fuel required for bang-bang control exceeds that required for impulsive control by a factor of 2. Another factor in the selection of a control approach and its associated performance parameters is the magnitude of the torques dictated by continuous control. For example, assuming a unit-step maneuver with $\kappa = -(\ln 0.05)/10 \approx 0.3$, the prescribed control torque at t_0^+ is approximately 6180 N-m. A control torque

Table 2 Two-pass aerocapture results

Pass no.	Peak accel., g	Peak q_c, W/cm^2	Total q_c, J/cm^2
1	−1.43	51.98	5384
2	−1.26	37.36	8063

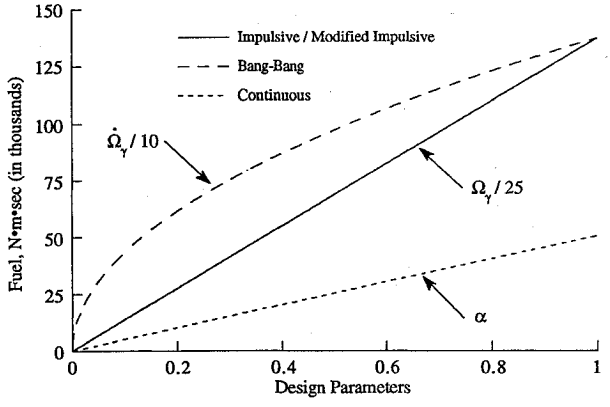

Fig. 8 Fuel comparisons for control techniques using unit-step input.

of this magnitude is prohibitively large within the context of this problem.

Based on the preceding discussion, the modified impulsive approach was best suited for application to aerocapture. Accordingly, throughout the remainder of the section, only the modified impulsive approach is considered. It should be pointed out, however, that all of the approaches display similar flight characteristics.

Two-Pass Aerocapture

The entry conditions in the first pass of the two-pass analysis were identical to those in the single-pass case except that the mid-corridor entry flight-path angle was −5.043 deg. In the first pass, the commanded bank angles were adjusted in order to target for a 360-min orbital period and 28.5-deg angle of orbit inclination. A minimization of the convective heating rate was also conducted. Assuming symmetry of the orbit, the velocity and flight-path angle at the exit of the first pass were used as entry conditions for the second pass. At the completion of the first pass the orbit was defined by an exit velocity of 9.937 km/s and a flight-path angle of 4.327 deg. These were the entry conditions in the second-pass simulation. The second-pass simulation was terminated by an orbit circularization burn at the 500-km altitude of the target orbit apogee.

Figures 9a–9l in conjunction with Table 2 illustrate the effects of two-pass aerocapture. Figures 9a and 9b display the bank-angle time histories for the first and second passes, respectively. Figures 9c and 9d show the altitude profiles for both passes. Note that on the second pass, the vehicle remains in the atmosphere longer, which results in higher total heating. Figures 9e and 9f show the velocity losses over the two passes, and Figs. 9g and 9h show the decelerations of the vehicle. The effect of the two-pass aerocapture as seen here is the greatly reduced deceleration of the spacecraft over the course of both aeropasses. The convective heating rates are illustrated in Figs. 9i and 9j, and the peak rates are given in Table 2. The peak heating rate in the first pass is on the order of 33% lower than in the single-pass case, and the second pass experiences a 52% decrease. Figures 9k and 9l show the total convective heating associated with each pass. Even though the two-pass case experiences a lower peak heating rate than the single-pass case, the total heating is greater by almost 74%. This higher total heating will require a thicker (and hence heavier) heat shield. The structural weight saving that results from the lower decelerations will, however, far exceed the weight increase due to the thicker heat shield. Another point to consider is that the ΔV required for orbit circularization in the two-pass case decreased by 30 m/s (≈18%) from the single-pass case.

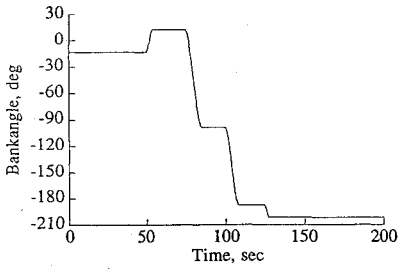

Fig. 9a Bank-angle history, first pass.

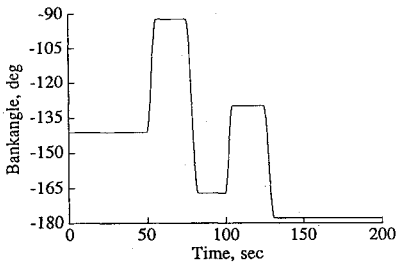

Fig. 9b Bank-angle history, second pass.

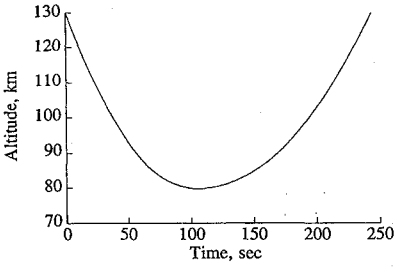

Fig. 9c Altitude history, first pass.

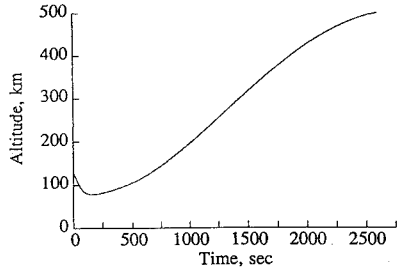

Fig. 9d Altitude history, second pass.

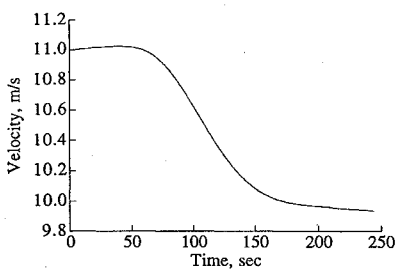

Fig. 9e Velocity history, first pass.

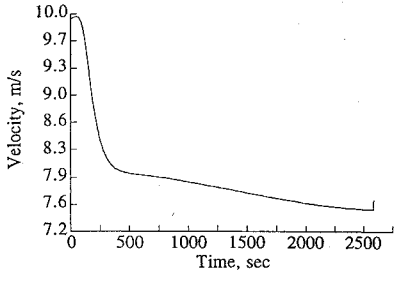

Fig. 9f Velocity history, second pass.

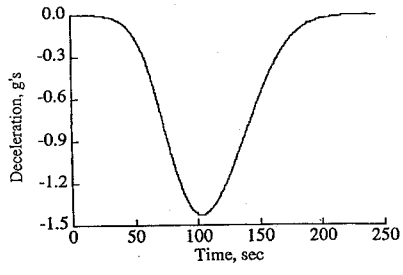

Fig. 9g Deceleration history, first pass.

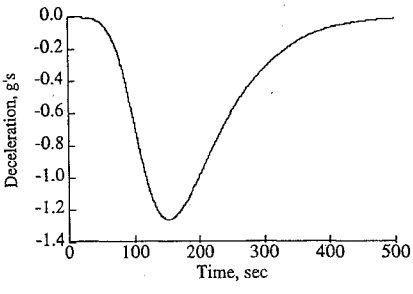

Fig. 9h Deceleration history, second pass.

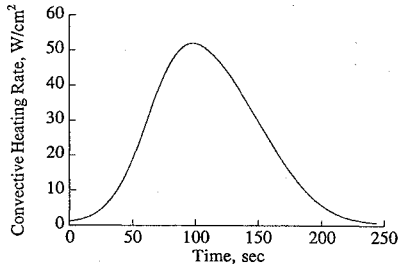

Fig. 9i Convective-heating-rate history, first pass.

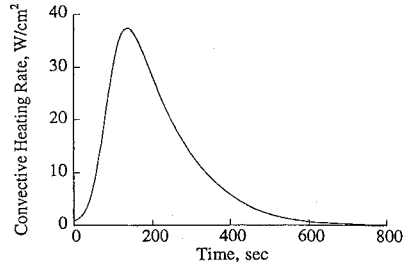

Fig. 9j Convective-heating-rate history, second pass.

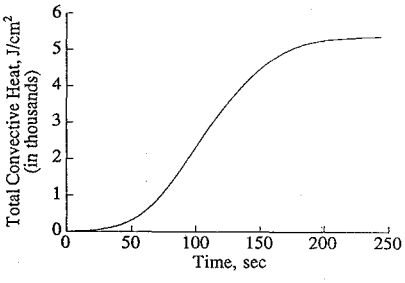

Fig. 9k Convective-heat-load history, first pass.

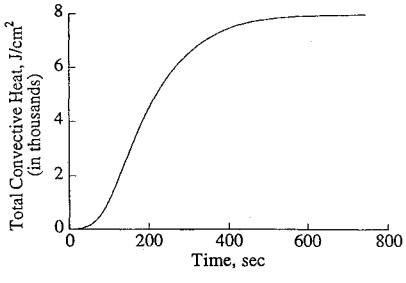

Fig. 9l Convective-heat-load history, second pass.

Discussion

This paper has presented four optimal-control problems applied to bank-angle control for lunar-return aerocapture. The first approach involves continuous control, which is implemented with control moment gyros, torque wheels, and throttlable reaction control jets. The second approach is suited to propulsive actuators and is in the form of bang-bang controls. Impulsive control is the third approach, where the control is in the form of impulses. The fourth approach is a modification of impulsive control where the impulses are replaced by pulses of finite magnitude and duration.

All of the approaches are applied first to a single-pass aerocapture problem, where POST was used to optimize the commanded bank angles so that the ΔV associated with orbit circularization was minimized. In each case, a successful series of commanded bank angles was determined such that the target parking orbit was achieved. The results from each case were then compared with the flight characteristics of an ideal bank-angle sequence. The peak deceleration never exceeded $4.65g$, the peak convective heating rates were in the vicinity of 80 W/cm^2, and the total convective heating was around 7600–7800 J/cm^2. In the case of continuous controls it was determined that the magnitude of the initial control forces required were unrealizable within the context of this problem. For identical maneuver times, the fuel required for a unit-step bank-angle modulation was twice as large for bang-bang control as it was for impulsive control. In the modified impulsive control, when impulse and pulse magnitudes were equated, the fuel and coasting angular velocities were identical to those found in impulsive control. However, the modified approach had a slightly larger maneuver time than the original impulsive approach. It was also demonstrated that if the various control approaches employed feedback about the ideal, or step-function, bank-angle sequence, atmospheric capture resulted, that is, each was unable to obtain the targeted exit conditions.

The modified impulsive-control approach was next applied to a two-pass aerocapture problem in order to evaluate the performance of a multipass technique. The peak convective heating rates for the first and second passes were decreased from the single-pass case by 33% and 52%, respectively. Also, the ΔV required to circularize the orbital trajectory upon arrival at apogee was decreased by 18%

from the single-pass case. A significant reduction in the deceleration was revealed for the two-pass case. The respective peak values for the first and second pass were $-1.43g$ and $-1.26g$ as compared to $-4.65g$ for the single-pass case. The only obvious drawback was that the total convective heating for the two-pass case increased from the single-pass case by 74%. In all likelihood, however, the structural weight saving that is enabled by the reduced g loading will far exceed the increase in heat-shield weight required to accommodate the higher total heating.

Conclusion

The following comments on the practical implementation of these control approaches are offered. As was mentioned in the Introduction, if atmospheric conditions could be precisely characterized, a simple ballistic trajectory could be flown such that the vehicle would not exceed design limitations and a prescribed target orbit would be obtained. In a dynamic environment, bank-angle modulation provides the necessary control required to safeguard mission objectives. Unfortunately, in the presence of atmospheric dispersions, aerodynamic mispredictions, and navigation errors, no bank-angle sequence can be predicted to acceptable tolerances. These uncertainties support the need for bank-angle control augmented with predictor-corrector techniques.

In this paper, the application of impulsive control has been successfully demonstrated in its application to aerocapture. Furthermore, in complementary efforts, it has been demonstrated that a predictor-corrector-augmented guidance algorithm can successfully negotiate inaccurately modeled flight conditions.[14–16] Impulsive bank-angle modulation in conjunction with predictor-corrector techniques can, in the presence of such uncertainties, successfully perform either single-pass or multipass aerocapture in a fuel-optimal manner.

Acknowledgments

This investigation was supported by the Mars Mission Research Center under NASA Grant NAGW-1331. The authors thank Richard W. Powell for his assistance in the implementation of the closed-loop control algorithms in POST.

References

[1]Repic, E. M., Boobar, M. G., and Chapel, F. G., "Aerobraking as a Potential Planetary Capture Mode," *Journal of Spacecraft and Rockets*, Vol. 5, No. 8, 1968, pp. 921–926.

[2]Walberg, G. D., "A Review of Aerobraking for Mars Missions," International Astronautical Federation, Paper 88-196, Oct. 1988.

[3]Tauber, M., Bowles, J., and Yang, L., "The Use of Atmospheric Braking During Mars Missions," AIAA Paper 89–1730, June 1989.

[4]Adams, A., Priest, C. C., and Sumrall, P., "Overview of Mars Transportation Options and Issues," AIAA Paper 90-3795, Sept. 1990.

[5]Walberg, G. D., "Aerocapture for Manned Mars Missions—Status and Challenges," AIAA Paper 91-2870, Aug. 1991.

[6]Braun, R. D., Powell, R. W., and Hartung, L. C., "Effect of Interplanetary Trajectory Options on a Manned Mars Aerobrake Configuration," NASA TP 3019, 1990.

[7]Finch, T. W., "Aerodynamic Braking Trajectories for Mars Orbit Attainment," *Journal of Spacecraft and Rockets*, Vol. 2, No. 4, 1965, pp. 497–500.

[8]Braun, R. D., and Powell, R. W., "Aerodynamic Requirements of a Manned Mars Aerobraking Transfer Vehicle," *Journal of Spacecraft and Rockets*, Vol. 28, No. 4, 1991, pp. 361–367.

[9]Freeman, D. C., Jr., Powell, R. W., and Braun, R. D., "Manned Mars Aerobrake Vehicle Design Issues," International Astronautical Federation, Paper 90-197, Oct. 1990.

[10]Boobar, M. G., Repic, E. M., and McDermott, A. M., "Approach and Entry Corridors for Aerobraking at Mars and Venus," *Journal of Spacecraft and Rockets*, Vol. 4, No. 5, 1967, pp. 682–684.

[11]Bourke, R. D., "SEI Engineering Requirements on Robotic Missions: Report of the Mars Atmosphere Knowledge Requirements Working Group," Jet Propulsion Laboratory, JPL Paper D-8465, April 1991.

[12]Willcockson, W. H., "OTV Aeroassist with Low L/D," *Acta Astronautica*, Vol. 17, No. 3, 1988, pp. 277–301.

[13]Walberg, G. D., "A Survey of Aeroassisted Orbit Transfer," *Journal of Spacecraft and Rockets*, Vol. 22, No. 1, 1985, pp. 3–18.

[14]Braun, R. D., Powell, R. W., and Lyne, J. E., "Earth Aerobraking Strategies for Manned Return from Mars," AIAA Paper 91-2873, Aug. 1991.

[15]Braun, R. D., and Powell, R. W., "Predictor-Corrector Guidance Algorithm for Use in High-Energy Aerobraking System Studies," *Journal of Guidance, Control, and Dynamics*, Vol. 15, No. 3, 1992, pp. 672–678.

[16]Powell, R. W., and Braun, R. D., "A Six-Degree-of-Freedom Guidance and Control Analysis of Mars Aerocapture," AIAA Paper 92-0736, Jan. 1992.

[17]Wingrove, R. C., "Trajectory Control Problems in Planetary Entry of Manned Vehicles," *Journal of Spacecraft and Rockets*, Vol. 2, No. 6, 1965, pp. 883–888.

[18]Schy, A. A., and White, J. A., "Deceleration Control System for Aerobraking and Skipout to Orbit at Mars," *Journal of Spacecraft and Rockets*, Vol. 6, No. 7, 1969, pp. 831–834.

[19]Gurley, J. G., "Guidance for an Aerocapture Maneuver," *Journal of Guidance, Control, and Dynamics*, Vol. 16, No. 3, 1993, pp. 505–510.

[20]Speyer, J. L., and Crues, E. Z., "Approximate Optimal Atmospheric Guidance Law for Aeroassisted Plane-Change Maneuvers," *Journal of Guidance, Control, and Dynamics*, Vol. 13, No. 5, 1990, pp. 792–802.

[21]McEneaney, W. M., "Optimal Aeroassisted Guidance Using Loh's Term Approximations," *Journal of Guidance, Control, and Dynamics*, Vol. 14, No. 2, 1991, pp. 368–376.

[22]Holmberg, N. A., Faust, R. P., and Holt, H. M., "Viking '75 Spacecraft Design and Test Summary," Vol. 1—Lander Design, NASA Reference Publication 1027, 1980.

[23]Brauer, G. L., Cornick, D. E., Olson, D. W., Petersen, F. M., and Stevenson, R., *Program to Optimize Simulated Trajectories (POST)*, Vols. I–III, Martin Marietta Corp., MCR-87-583, NAS1-18147, Sept. 1987.

[24]Anon., *U.S. Standard Atmosphere*, National Oceanic and Atmospheric Administration, National Aeronautics and Space Administration, United States Air Force, Oct. 1976.

[25]Sutton, K., and Hartung, L. C., "Equilibrium Radiative Heating Tables for Earth Entry," NASA TM 102652, May 1990.

[26]Chapman, D. R., An Approximate Analytical Method for Studying Entry into Planetary Atmospheres, NACA TN 4276, 1958.

[27]Silverberg, L., "Uniform Damping Control of Spacecraft," *Journal of Guidance, Control, and Dynamics*, Vol. 9, No. 2, 1986, pp. 221–226.

[28]Bryson, A. E., Jr., and Ho, Yu-Chi, *Applied Optimal Control*, Hemisphere, Washington, 1975.

[29]Redmond, J., and Silverberg, L., "Fuel Consumption in Optimal Control," *Journal of Guidance, Control, and Dynamics*, Vol. 15, No. 2, 1992, pp. 424–430.

[30]Redmond, J., and Silverberg, L., "On the Fuel Optimal Reorientation of Axisymmetric Spin-Stabilized Satellites," *Journal of Guidance, Control, and Dynamics*, Vol. 16, No. 1, 1993, pp. 217–219.

[31]Silverberg, L. M., and Redmond, J. M., "A Unified Numerical Approach for the Exact Solution of Fuel and Time Optimal Control of Linear Systems," *Journal of Guidance, Control, and Dynamics* (submitted for publication).

[32]Silverberg, L. M., and Meyer, J. L., "Fuel Optimal Slewing of an Experimental Hinged-Free Beam," *Journal of Guidance, Control, and Dynamics*, Vol. 16, No. 6, 1993, pp. 1162–1168.